A continuous high-throughput bioparticle sorter based on 3D traveling-wave dielectrophoresis†

I-Fang Cheng,[a] Victoria E. Froude,[b] Yingxi Zhu,[b] Hsueh-Chia Chang*[b] and Hsien-Chang Chang*[acd]

We present a high throughput (maximum flow rate ~10 μl/min or linear velocity ~3 mm/s) continuous bio-particle sorter based on 3D traveling-wave dielectrophoresis (twDEP) at an optimum AC frequency of *500 kHz*. The high throughput sorting is achieved with a sustained twDEP particle force normal to the continuous through-flow, which is applied over the entire chip by a single 3D electrode array. The design allows continuous fractionation of micron-sized particles into different downstream sub-channels based on differences in their twDEP mobility on both sides of the cross-over. Conventional DEP is integrated upstream to focus the particles into a single levitated queue to allow twDEP sorting by mobility difference and to minimize sedimentation and field-induced lysis. The 3D electrode array design minimizes the offsetting effect of nDEP (negative DEP with particle force towards regions with weak fields) on twDEP such that both forces increase monotonically with voltage to further increase the throughput. Effective focusing and separation of red blood cells from debris-filled heterogeneous samples are demonstrated, as well as size-based separation of poly-dispersed liposome suspensions into two distinct bands at 2.3 to 4.6 μm and 1.5 to 2.7 μm, at the highest throughput recorded in hand-held chips of 6 μl/min.

Introduction

Selective manipulation and rapid separation of living cells and vesicles/liposomes are integral to future medical diagnostics and drug synthesis applications. Conventional processes for distinguishing bacteria and cell types employ time-consuming laboratory techniques such as cell culture or flow cytometry using magnetic-activated cell sorting (MACS)[1,2] or fluorescence-activated cell sorting (FACS).[3,4] MACS uses antibody labeled magnetic beads for cell separation. Although it can achieve large volume sorting, low and variable product purity remains major shortcomings. The fluorescence-activated cell sorting (FACS) method screens labeled-cells with high purity but at low throughput if sorting of multiple cells is required.

Label-free sorting with microfluidic devices may extend high-purity sorting to a larger mixture of cells, as multi-stage sorting can be easily implemented on a portable chip, with dimensions less than 4 × 4 cm². One particular microfluidic cell sorting technique, that is both cell-sensitive and non-damaging, is AC dielectrophoresis (DEP).[5–14] Although DC dielectrophoresis is

possible in theory, the propensity for bubble-generating electrolysis reactions of micro-electrodes with a constant DC current eliminates their use for effective on-chip DC DEP sorting. AC DEP is the motion of a particle due to a time-averaged electrokinetic particle force that results from a particle dipole, whose magnitude is based on the relative permittivity/conductivity of the particle to that of the surrounding medium, induced by an AC electric field. The particle travels towards (positive DEP) or away (negative DEP) from high field regions when the particle is more or less polarized than the surrounding medium, respectively. Most particles exhibit different DEP mobility directions at different frequencies, with one or two distinct cross-over frequencies when the mobility changes sign. Other than the relative conductivity and permittivity, the direction of DEP mobility at a particular frequency is also sensitive to the cell size/shape and the protein density on the cell membrane, which vary widely for different species and are distinct for live/dead and diseased/healthy bacteria/cells.[5–9] Recent studies suggest that surface conductance change due to differences in the density of charged functional groups and the number of docked charged molecules can also affect the sign and magnitude of the DEP mobility.[8,9] With various sorting electrodes on a chip at different AC frequencies, DEP hence offers a high-sensitivity, label-free and multi-separator sorting platform.[10,11] For instance, bacteria have been effectively separated into different downstream channels based on bacteria type or viability.[5] Another continuous-flow DEP sorting design uses negative DEP instead of gravity in field-flow fractionation (DEP-FFF).[12] Negative DEP force provides a repulsive force that pushes particles with different negative DEP mobility away from the underlying electrodes onto different streamlines with different residence times. However, with the small velocity gradient offered by

[a] *Institute of Nanotechnology and Microsystem Engineering, National Cheng Kung University, Tainan, Taiwan, ROC. E-mail: hcchang@mail.ncku.edu.tw*
[b] *Center for Microfluidics and Medical Diagnostics, Department of Chemical and Biomolecular Engineering, University of Notre Dame, Notre Dame, Indiana, 46556, USA. E-mail: hchang@nd.edu*
[c] *Institute of Biomedical Engineering, National Cheng Kung University, Tainan, 701, Taiwan, ROC*
[d] *Center for Micro/Nano Science and Technology, National Cheng Kung University, Tainan, 701, Taiwan, ROC*
† Electronic supplementary information (ESI) available: Video S1, RBC and bacteria sorting; Video S2, voltage–velocity variations; and Video S3, liposome sorting. See DOI: 10.1039/b910587e

a microfluidic device, the FFF separation range is limited and a long (30 cm) separation channel is required, which severely hampers device portability.

The most efficient continuous-flow DEP sorting design is based on the difference in the DEP mobility direction,[6,11] rather than the mobility difference, as the latter is limited to small finite-volume samples.[12] Such continuous sorting is typically done with three-dimensional AC electric fields sustained between long and narrow (100 micron) sorting electrode pairs (DEP gates) on the top and bottom sides of a closed chip that obliquely span the width of the open-flow channel.[13–16] The main flow channel that houses these DEP gates bifurcates or trifurcates into two or three divided sub-channels downstream, into which the particles will be sorted. Particles are focused upstream of the sorting region into a 10-micron region in the middle of the channel by two side arrays of electrodes that operate at a negative DEP frequency for all particles. Those with negligible DEP mobility near the cross-over frequencies can pass the DEP gates and are convected into the middle sub-channel downstream. Those with negative DEP mobility cannot pass the DEP gates and instead slide along the slanted gates to the two sides of the channel and are convected into side sub-channels. Secondary sorting can be carried out in each of the sub-channels into higher-generation channels downstream in a multi-stage design. Negative DEP traps, operated at different frequencies at the downstream channels, can trap the sorted particles and quantify them by impedance sensing. An integrated 3D DEP chip for continuous filtering, focusing, sorting, trapping and detection of three types of bacteria was reported in our earlier paper.[16]

Although DEP gates do not impart a force on the liquid and hence produces no hydrodynamic resistance, the throughput of DEP chips is still lower than flow cytometry, with a linear velocity that does not exceed 300 microns/s. The key reason is that the DEP force is weak and sorting at a localized DEP gate is ineffective at high flow rates. For reasonably sized portable chips about 2 cm long, 1 mm wide and 25 microns high, the maximum flow rate reported thus far is 1 μl/min,[16] which is impractical for rapid diagnostic applications with 100 μl sample volumes. Even with a low linear velocity, higher flow rates can be achieved with larger chips but the chips would not be portable. The DEP-FFF chip requires a long channel for particles to sample the entire span of streamlines across the gap, typically 30 cm long for micron-sized cells.[12] There is hence a need to extend the high-precision, continuous DEP sorting chip platform to high throughputs beyond 1 μl/min and for a typical portable chip with dimensions smaller than 4×4 cm^2.

All earlier DEP chips use a design that exploits the force at a single electrode DEP gate due to coupling between the in-phase components of the electric field and the induced particle dipole, which will be termed conventional dielectrophoresis. The conventional DEP forces on the particles are either in the direction (positive DEP) or against the direction (negative DEP) of the drag force provided by the flow, with the negative DEP force necessary larger than the drag. If the DEP force is normal to the flow direction, the latter constraint can be removed to allow a higher flow rate. However, a higher flow rate would imply a smaller net DEP force a particle will experience in its shorter transit time across the localized DEP gates. It would hence be desirable to have an array of digitated electrodes spanning both the width and length of the entire channel to produce a larger net force on the particle during its residence time on the chip.

DEP forces created by applying a train of traveling-wave (tw) electric fields along a row of electrodes offer all the above features: large net particle force normal to the flow direction. The DEP particle force is, however, different from conventional DEP. The particle dipole reorients as it traverses each electrode. As the dipole relaxation time is different from the field rotation period seen by the particle, a particle force is imparted by the out-of-phase component of the tw field (relative to the particle dipole) to create linear particle motion along the direction where the phase increases or decreases. Masuda et al. proved that three phase voltages in the frequency range between 0.1 Hz and 100 Hz could be used to induce controlled particle linear translation normal to the electrode length.[17] In the low frequency range, the particle motion was dominated by electrophoresis, producing particle separation based on particle size (DEP) and net charge (electrophoresis). Fuhr et al. presented DEP dominated particle linear motion by using a four phase shift traveling wave field with a frequency range between 10 kHz to 30 MHz.[18] Theoretical analysis has shown that the translational force experienced by a particle undergoing twDEP depends on several factors[19–21] which allow for effective manipulation and separation of cells by exploiting twDEP behavior.[22–24] Morgan et al. developed a multi-layering microelectrode technique to fabricate large area twDEP devices,[25,26] whereby a chip with a 1000 microelectrode array needs only 4 connecting pads. The twDEP design has been exploited by X-B Wang et al. in a spiral electrode design, with only 4 connecting pads, to manipulate and concentrate human breast cancer cells.[27] The cells are induced to move toward the center or periphery of the spiral electrode. R. Pethig et al. have improved the sensitivity and purity of cell separation by enhancing twDEP with signal superposition.[28]

However, the high-throughput advantage of twDEP has not been optimized in the past designs, which involve either separation without netflow or twDEP force parallel to the drag force. This paper presents a continuous particle-sorting device that combines 3D DEP focusing with large-array 3D twDEP sorting, where the twDEP particle force is perpendicular with the flow direction and is sustained over a large length of the chip. With particle flow parallel to face-to-face ladder-shaped electrodes, 3D negative DEP focusing provides the same starting position for all particles focused into a particle queue in the middle of the channel. As the focused particle stream enters the traveling-wave electrode array, the particles will move along the direction parallel to the traveling-wave: towards the upper side of the channel wall if they experience positive twDEP and vice-versa. Therefore, particles with different sizes, dielectric properties, and shapes develop different traveling velocities or directions, resulting in the sorting of particles to different downstream sub-channels at high throughputs (flow rate ~10 μl/min or linear velocity ~3 mm/s). The repelling force of negative DEP is also designed into the chip to ensure that the particles are far from the electrodes, avoiding particle adhesion due to sedimentation. However, this negative DEP effect can reduce the twDEP force if the electrode arrays are fabricated on one surface, as the repelled particles would feel a weaker field. We hence choose a 3D electrode array design.

In anticipation of future platforms with parallel sorters, a twDEP sorter normal to the flow offers a clear instrumentation

advantage over other continuous-flow DEP sorters. Realistic samples contain many different types of bacteria to be sorted and with the localized DEP gate, the sorting can only be achieved if the sorted particles are on opposite side of the cross-over, the sorting is based on the difference in mobility direction. Consequently, each DEP sorting gate must be operated at a different frequency, with a separate input signal. In contrast, the twDEP design in the current chip, with the DEP force normal to the flow direction, sorting can be based on the difference in the DEP mobility magnitude, as well as the mobility direction. It is hence possible to apply a single set of 4 phase-shift input signal to induce transverse separation of many particles, based on the differences in their twDEP mobility magnitude and directions, into several outlet channels downstream to achieve continuous fractionation of a spectrum of DEP mobilities on both sides of the cross-over, with a high linear velocity unmatched by DEP-FFF because of the sustained twDEP along the chip.

To our knowledge, a high-throughput 3D twDEP normal sorter with a focusing and anti-sedimentation DEP design has not been reported in the literature.

Theory and design

We review the theory on twDEP below to guide our design.[29,30] The time-dependent dielectrophoretic force acting on a particle, due to the presence of an induced particle dipole with dipole moment $\vec{m}(t)$ by an electric field $\vec{E}(t)$ is given by $\vec{F}(t) = (\vec{m}(t)\cdot\nabla)\vec{E}(t)$ or without the vector notation,

$$F(t) = 2\pi\varepsilon_m r^3[Re(f_{CM})\nabla E^2 + Im(f_{CM})(E_{x0}^2\nabla\varphi_x + E_{y0}^2\nabla\varphi_y + E_{z0}^2\nabla\varphi_z)]$$

where r is particle radius, ε_m is the permittivity of the surrounding medium, E is the intensity of the applied electric field, and the subscript 0 refers to the uniform part of the field which is gradient free. The key parameter is the Clausius-Mossotti (CM) factor

$$f_{CM} = \frac{\varepsilon_p^* - \varepsilon_m^*}{\varepsilon_p^* + 2\varepsilon_m^*} \tag{1}$$

where ε_p and ε_m are the permittivity of the particle and the surrounding medium, respectively. $Re[f_{CM}]$ and $Im[f_{CM}]$, the real and imaginary parts of the Clausius-Mossotti factor respectively, give the in-phase and out-of-phase component of the dipole moment.

$$Re[f_{CM}] = \frac{(\varepsilon_p - \varepsilon_m)(\varepsilon_p + 2\varepsilon_m) + \left(\frac{\sigma_p - \sigma_m}{\omega}\right)\left(\frac{\sigma_p + 2\sigma_m}{\omega}\right)}{(\varepsilon_p + 2\varepsilon_m)^2 + \left(\frac{\sigma_p + 2\sigma_m}{\omega}\right)^2}$$

$$Im[f_{CM}] = \frac{(\varepsilon_p - \varepsilon_m)\left(\frac{\sigma_p + 2\sigma_m}{\omega}\right) - (\varepsilon_p + 2\varepsilon_m) + \left(\frac{\sigma_p - \sigma_m}{\omega}\right)}{(\varepsilon_p + 2\varepsilon_m)^2 + \left(\frac{\sigma_p + 2\sigma_m}{\omega}\right)^2} \tag{2}$$

The time average force of conventional dielectrophoresis on a particle of size r is then

$$F_{DEP} = 2\pi r^3\varepsilon_m Re[f_{CM}(\omega)]\nabla E^2 \tag{3}$$

The frequency dependent real part of CM factor determines if the particle is attracted to $(Re(f_{CM}(\omega)) > 0)$ or repelled from $(Re(f_{CM}(\omega)) < 0)$ the high field region. In our focusing portion of the device, the DEP force near the electrode pair can be given in dipole approximation (perpendicular to the boundary of the capacitor) as[13,14]

$$F_{DEP} = \frac{27}{32}\pi^2\varepsilon_m\left(\frac{r^3}{a^3}\right)Re[f_{CM}(\omega)]V_{rms}^2 \tag{4}$$

where a is the channel height and V_{rms} is the root-mean-square potential.

The out-of-phase imaginary component $Im[f_{cm}(\omega)]$ of the Clausius-Mossotti is due to the difference in the charge relaxation times between the particle and the suspending medium in a phase-shifted AC electric field. A positive out-of-phase component indicates that the dipole moment of the particle lags behind the electric field. Depending on whether the sign of $Im[f_{cm}(\omega)]$ is positive or negative, the resulting force causes the linear motion of particles to move either along the co-field or anti-field directions.

Since our electrodes are equally spaced, the phase angle change across each electrode is the same. The tw field is then just the applied voltage divided by λ, the wavelength of the traveling field which is also the distance between every fourth electrodes. The traveling-wave dielectrophoretic force (twDEP) acting on a particle in the electric field is then given by[20,21]

$$F_{TWD} = -\frac{4\pi^2\varepsilon_m r^3}{\lambda}Im[f_{CM}(\omega)]E^2 \tag{5}$$

The twDEP force is hence inversely proportion to λ and the smallest possible spacing of the electrodes relative to the particle size should be designed to effectively manipulate the particles. The limiting values of the real and imaginary parts of the CM factor are −0.5–1 and −0.75–0.75 respectively, by taking the limits of the expressions in (2) for ω approaching zero and infinity, corresponding to conductive and dielectric polarization. The real part monotonically approaches its limiting values at low and high frequencies, while $Im[f_{CM}(\omega)]$ approaches zero at the same limits, giving rise to a sharp maximum at a resonant frequency. There are two conditions for stable traveling wave dielectrophoretic movement: when the real component of CM factor is kept negative to produce a repulsive force by negative DEP to ensure that the particles are levitated from the electrodes, and when the imaginary component is close to the maximum such that the corresponding twDEP force can induce motion along or opposing the traveling wave electric field.

Balancing the traveling wave dielectrophoretic force with viscous drag for a particle of size r in a medium with viscosity η provides the linear twDEP particle velocity normal to the through-flow

$$v_{TWD}(x) = -\frac{2\pi\varepsilon_m r^2}{3\lambda\eta}Im[f_{CM}(\omega)]E^2 \tag{6}$$

and the characteristic time for separation with maximum through-flow linear velocity can then be estimated. Maximum separation occurs when a particle with zero twDEP velocity is separated from one with velocity (6) during the residence time of the particles within the twDEP array, which is determined by the through-flow linear velocity u_{max}. A smaller residence time would

provide a larger throughput but less separation. A larger residence time would reduce the throughput. Hence, the maximum throughput velocity with maximum separation can be estimated to be

$$t = w_h/v_{TWD}(x) < l/u_{max} \qquad (7)$$

where l is the length of the traveling wave electrode array and w_h is the half width of the channel. For reasonable values of $\lambda = 100$ μm, $r = 6$ μm, $l = 1$ cm and $w = 0.1$ cm in our chip, we obtain u_{max} of 3.5 mm/s and a maximum throughput of 10 μl/min. This linear velocity is an order of magnitude larger than that for a DEP-FFF chip,[12] the fastest DEP unit reported, with typical u_{max} values ranging from 300 μm/s to 500 μm/s for red blood cells.

Above the MHz frequency range, the non-uniform electric field creates a thermal gradient and an electro-thermal current is generated, especially with high conductivity solutions and high applied voltage, termed the electro-thermal effect. This effect is not only strongly dependent on the applied voltage and the conductivity of the medium, but also on the electrode area and the geometry. Electro-thermal effects could damage the cells by inducing cell lysis, change the electric properties of the cells, or induce a thermal flow of cells that would dominate the DEP force being applied. In our experiment, high frequency was avoided when using a high conductivity medium to avoid electro-thermal effects.

Experimental section

Microfabrication

As shown in Fig. 1, Au/Cr electrodes (200 nm/30 nm thick) were deposited on a glass slide (Kimble, 76 mm × 26 mm and 1 mm thick) by an electro-beam evaporator (E-beam VT1-10CE, ULVAC). Positive photoresist (AZ 5214) was spin-coated on the deposited metal layer and patterned by standard photolithography techniques with the electrode geometry. The metal layer was then etched and the remaining photoresist removed. An electrode width and gap size of 12.5 μm was chosen, such that a significant field gradient exists across the blood cells and other micrometer-sized bioparticles. After electrode patterning, a negative photosensitive epoxy-based photoresist, SU 8-25, was spin-coated on one of the electrode-patterned slides. Following standard lithography techniques of exposure and developing, a channel was patterned into the SU 8-25 with a height of 25 μm, a width of 1 mm, and a length of 1.3 cm. The inlet and outlet holes were drilled by a diamond drill into a second electrode-patterned slide. The fluidic inlet and outlet ports were located at the ends of the microchannel. The alignment marks were defined in the microelectrode and microchannel fabrication steps. A UV curable adhesive glue (LOCTITE 3492) with a viscosity of 300–500 Cp was spin-coated onto the slide with the SU 8 layer, leaving a 2–3 μm thick coating of glue. The two face-to-face chips were aligned and pressed together using by a mask aligner containing a three axis moving platform (Karl Suss MA6) with micrometer precision movement. After alignment and pressing together, the chip was exposed to UV light to cure the bonding layer of the two slides that glued the two slides together. The adhesive glue has good coverage, high bonding strength, and a small adhesive thickness. Typical thickness of the bonding layer
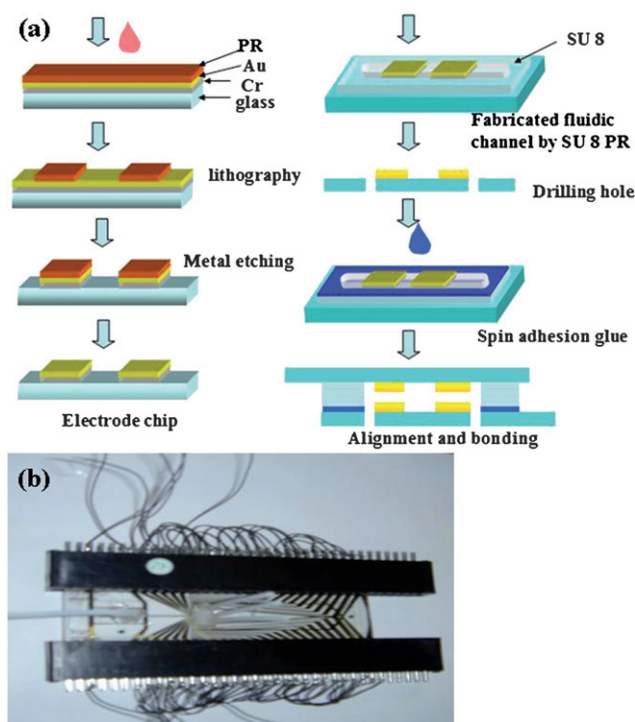

Fig. 1 (a) Schematic of the microfabrication process using standard lithography techniques to fabricate a microelectrode and a microchannel. UV bonding is used to bond the two electrode slides. (b) Photograph of the finished chip. The working channel within the chip is 1.3 cm long, 1 mm wide and 25 microns high. The entire chip is about 4 × 2 cm² in area.

was less than 1 μm after being laminated. The connecting pads of the 3D chip were inserted into two ISA bus sockets, and the same phase electrode was connected to each with ISA bus. The finished chip was inserted into two ISA slots to reduce wire bonding processing to every chip. An image of the fabricated chip is shown in Fig. 1(b) with its dimensions indicated in the figure caption.

System configuration

An applied function generator (WAVETEK 195) was used to reach an output voltage range of 5 mV$_{p-p}$ to 20 V$_{p-p}$ with a frequency range of 0 to 16 MHz and an output of four different signals simultaneously with phase control. The suspension of particles was placed into a 500 μl microsyringe (Hamilton 81220) and the fluidic injection and collection was accomplished via Teflon tubing (inside diameter = 0.5 mm, outside diameter = 1.5 mm). The sample was injected continuously into the microchannel by a microsyringe pump (KDS 230) through a Teflon tube. The experiment was observed through an inverted microscope (Olympus CH 40) and videos and photos were recorded by a high speed CCD camera (60 frames/s, Q Image). Cell motion velocity was determined by measuring the time taken for individual cells to move a given distance, with a time interval of 0.2 s/frame. Average cell velocities were determined for 3 individual cells as a function of the applied voltages and frequencies.

The 3D DEP focusing electrode was arranged in front of the twDEP separation electrode to produce a small particle stream

that provided the same starting position for all particles. The twDEP separation electrode was perpendicular to the flow direction, as shown in Fig. 2(a). The amplitudes of applied voltages ranged from 2 V_{p-p} to 16 V_{p-p} at the frequency range of 100 kHz to 10 MHz. The electrode arrangement of 3D DEP focusing and the applied phase of each electrode are shown in Fig. 2(b). Fig. 2(c) shows a traveling electric field was applied by sinusoidal AC voltage with a sequential 90 degree phase shift to each electrode and each is exactly out of phase (180 degree difference) with its complementary electrode on the opposite layer. The face-to-face electrode array is arranged on the top and bottom slides of the channel. Each electrode of the array is 1 cm in length and 12.5 μm in both width and gap spacing. The microchannel is 1 mm wide, 1.3 cm long and 25 μm high.

Sample preparation

The 280 mM D-mannitol solution used is an isotonic solution with low conductivity. It was mixed with 1X PBS solution (137 mM NaCl, 2.7 mM KCl, 4.3 mM Na_2HPO_4, 1.47 mM KH_2PO_4, pH = 7.4) in an 11:1 ratio to control the conductivity of the experimental buffer, giving a final conductivity of the experiment buffer of 1.2 mS/cm. The red blood cells (RBC) were diluted 1000 fold and suspended in the isotonic experiment solution giving a final cell concentration of ~10^6 cells/ml. The size of the erythrocytes approached 5 μm–8 μm. *Staphylococcus aureus* (*S. aureus*, BCRC 14957) was cultured on Tryptic Soy Agar (TSA) at 35 °C. We also mixed *S. aureus* and RBCs in this solution, taking care to maintain the bacteria concentration at 10^8 CFU/ml. Both the RBC and the *S. aureus* samples are obtained by our collaborator at the Department of Medical Laboratory Sciences and Biotechnology at the National Cheng Kung University at Tainan, Taiwan (see ref. 16 for more details on sample preparation).

Other than sorting different bioparticles (bacteria or cells), the twDEP sorter is also capable of sorting the same species of different size, as both the real and imaginary parts of the Clausius-Mossotti factor f_{CM} in (2) for cells with bilayer membranes can be size dependent.[8,9] We demonstrate this size-sorting capability with a polydispersed liposome population with a large size range—liposomes with lipid bilayer membranes are good models of cells. Liposomes were synthesized *via* the commonly used extrusion technique using a 10:1 ratio of 1,2-dioleoyl-*sn*-glycerol-3-phosphate (DOPA) to 1,2-dioleoyl-*sn*-glycero-3-phosphoethanolamine-N-(7-nitro-2-1,3-benzoxadiazol-4-yl) (DOPE) as described in detail elsewhere.[31] The two lipids in a DOPA:DOPE powder weight ratio of 10:1 were well mixed in deionized water (Barnstead Nanopure II) after being stirred at 600 rpm for 24 h at room temperature. The suspension of hydrated lipids was subsequently extruded repeatedly 5 times through a microextruder (Avinti Polar lipids) with a polycarbonate filter of 1 μm pore diameter. Initially, liposome suspensions had a polydispersity of 0.165 and a radius of $r = 140 \pm 23$ nm. Over time, liposome instability initiates fusion, creating larger vesicles as well as increasing the number of lamella per liposome with increased aging time, as reported in previous studies.[32] All samples used in these experiments were aged at room temperature for at least two weeks, increasing the number of multi-lamellar vesicles as well as the average size and polydispersity of samples. The average liposome radius and size distribution were determined by dynamic light scattering (Brookhaven Instruments, ZetaPALS) both before and after sorting. Aged liposome samples, before sorting, show a marked increase in their size distribution. Large vesicles (>1–2 μm) appear in both unilamellar and multilamellar forms created through the previously described fusion of the unstable smaller vesicles, and some of the smallest vesicles (≤ ~500 nm), corresponding to the original vesicles, still remained in the solution.

Results and discussion

As described previously, the traveling wave velocity of particles is frequency dependent; therefore, the migration velocity of RBC was measured as a function of the frequency of the applied field under a specific voltage. RBCs were suspended in a medium with a conductivity of 1.2 mS/cm. At frequencies above several hundred kHz, the applied field gradually penetrated through the plasma membranes, leading to a decrease in Re[f_{CM}] and an increase in Im[f_{CM}] with frequency such that their velocities v_{TWD} increased.[22] Red blood cells experienced negative DEP when the applied frequency was below 650 kHz. At a frequency below 200 kHz, particles underwent strong negative DEP and weak twDEP force, such that particles were captured in the electrode gap. Fig. 3(a) shows that with an applied voltage of 12 V_{p-p} at a frequency of 200 kHz, RBCs experience strong negative DEP and move along a co-field direction by twDEP force, resulting in RBC trapping at the left hand side of the electrode array and allowing only approximately 20% of the RBCs to be transported through the electrode array. Theoretically,[8] at frequencies above MHz, the applied field will penetrate through plasma membranes into the conducting cell interior, leading to Re[f_{CM}]>0; thus, the
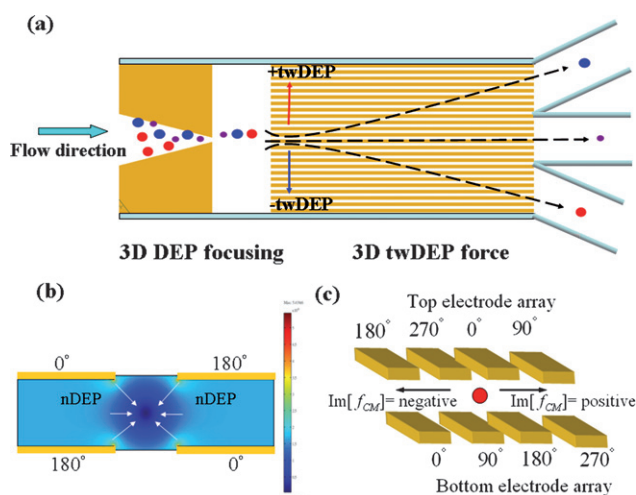

Fig. 2 Schematic diagram of the 3D electrode design. (a) Top view of electrode structure, particles experience different directions or different velocities of twDEP which transport them into relative outlets. (b) Side view of electrode structure depicting particles being repelled away from the electrode by nDEP and (c) transported in different directions depending on the imaginary part of their CM factors.
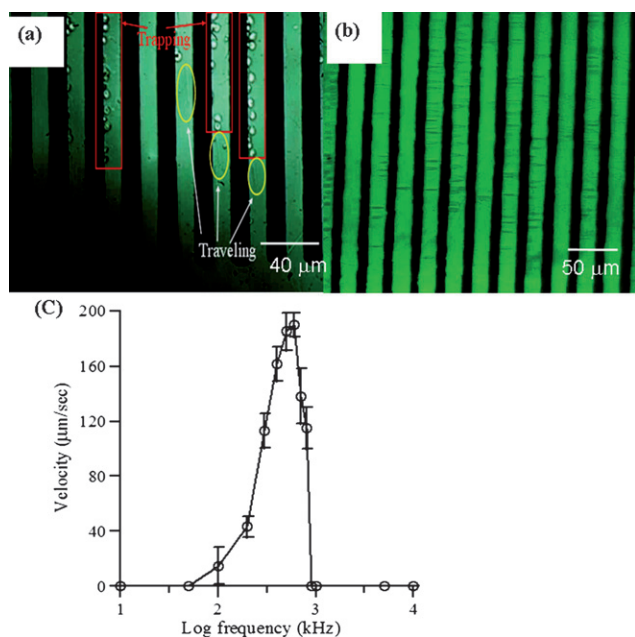
Fig. 3 (a) When applying 12 V_{p-p} at a frequency of 200 kHz, RBCs experience strong negative DEP and were trapped at the right hand side of the electrode. (b) When applying 12 V_{p-p} at a frequency of 800 kHz, RBCs experience strong positive DEP that stretches and traps them at the electrode edge. (c) Experimentally determined traveling-wave velocity dependence on frequency, where the transverse migration velocity of the blood cells is measured as a function of the frequency under 12 V_{p-p} applied. In a narrow frequency range of 300 kHz to 650 kHz, the red blood cells (RBC) migrated along the co-field direction (data are averaged over three runs).

cells are trapped at the electrode edges by positive DEP forces, and their velocities, v_{TWD}, reduce to zero. When frequency was increased above 700 kHz, RBCs were gradually attracted to the electrode edge, demonstrating pDEP phenomenon, especially at frequencies higher than 800 kHz. As shown in Fig. 3(b), RBCs experience strong positive DEP and were stretched between the two electrodes, at field parameters of 12 V_{p-p} and 800 kHz. This phenomenon could be exploited in cell immobilization and drug immersion. We observe that, throughout a narrow band of frequencies, ranging from 300 kHz to 650 kHz, RBCs were rotating and traveling along the co-field direction, with the maximum velocity of twDEP translation occurring near 500–600 kHz, as depicted in Fig. 3 (c). Above 800 kHz, twDEP force no longer dominates the weaker DEP force and particles were stretched and trapped at the electrode by the combined twDEP and conventional DEP forces.

We also optimized the particle velocity of individual cells as a function of the magnitude of the applied signals. As the voltage varied from 2 V_{pp} to 16 V_{pp}, at a fixed field frequency of 500 kHz, the cells migrated along the co-field direction with velocity increasing as a function of increasing voltage (see video in Supplementary Material,† *voltage–velocity variations.MP4*). In our experiments, results demonstrated a voltage–velocity profile with a roughly square relationship when the applied voltage is below 14 V_{p-p}, as shown in Fig. 4. In comparison, previous twDEP studies report much weaker voltage-dependence at higher voltages.[24,27] With their two-dimensional electrode array
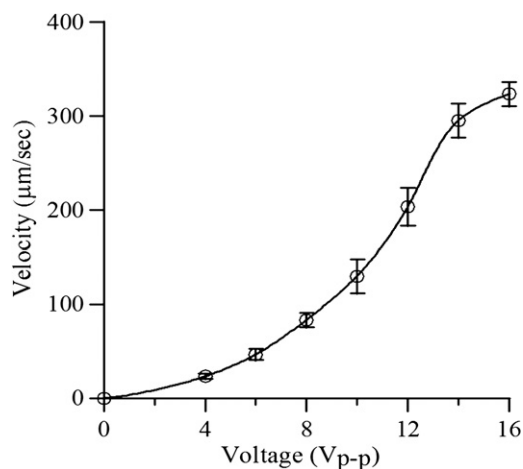

Fig. 4 The experimentally determined traveling-wave velocity–voltage profile demonstrated an approximately square relationship of blood cell traveling velocity with applied voltage when the applied voltage is lower than 14 V_{p-p} (data are averaged over three runs).

on one surface in these studies, this quadratic scaling breaks down when cells are levitated out of the strong field region by negative DEP. Therefore, the saturation point of voltage for their design, where the velocity no longer increases with the square of voltage, is at 3 V_{p-p} with v_{TWD} of approximately 25 μm/s under these conditions.[27] In our experiment with 3D electrode arrays, the saturation point of the voltage is about 3 times higher than the 2D twDEP electrode array, and the migration velocity is approximately one order of magnitude greater than 2D twDEP. For blood cells, we are able to achieve a maximum of 3 mm/s and 10 μl/min for the linear velocity and throughput of the flow, respectively, and still achieve separation.

To obtain a linear flow velocity of 200 μm/s, a voltage of 12 V_{p-p} at a frequency of 500 kHz was applied on the twDEP electrode array. Fig. 5 shows the moving trajectories for multiple particles, where particle velocities with flow direction are $u \sim 100$ μm/s, 250 μm/s, 600 μm/s and 1 mm/s respectively, when a voltage of 12 V_{p-p} at a frequency of 500 kHz was applied on the twDEP
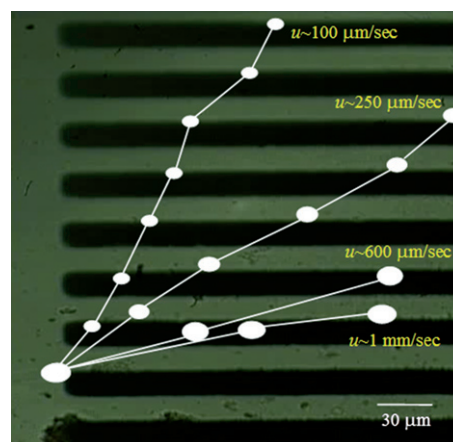

Fig. 5 Different moving trajectories and particle velocities with flow direction are depicted when a field with an ac voltage of 12 V_{p-p} and a frequency of 500 kHz was applied to the twDEP electrode array.

electrode array. They experience traveling field force with different applied flow velocities that demonstrated different deflection angles.

As is evident in Fig. 6 (a), the cells are randomly distributed in front of the electrode array. An AC voltage of 14 V_{p-p} at a frequency of 500 kHz was applied on the twDEP electrode array with a linear flow velocity of 2 mm/s (flow rate∼6 µl/min). At 4 mm along the electrode array the particles are being transported along the co-field direction with roughly a 10 degree angle of deflection, as depicted in Fig 6 (b), with an average twDEP velocity approaching 250 µm/s. At 8 mm along the electrode array, almost all the cells were transported to the upper side wall of the channel and sorted to the upper sub-channel, as shown in Fig. 6 (c) and (d). This result suggests that the twDEP characteristic time of the particles across the electrode array is longer than the residence time of the particles, such that they transverse the entire width and length of electrode array to achieve maximum separation.

We also sorted the blood cells from a mixed sample with *S. aureus*. The particle focusing electrode employed an applied voltage of 24 V_{p-p} and a frequency of 500 kHz with a flow velocity of 1.3 mm/s or a flow rate of 4 µl/min. The twDEP electrode array used an applied voltage of 12 V_{p-p} and a frequency of 500 kHz. Under these conditions, the bacteria and blood cells can be focused into a narrow particle stream (Fig. 7 (a)). When the particles enter into the twDEP electrode array, blood cells experienced higher twDEP force transporting them toward the upper sub-channel, and the bacteria experience a lower twDEP force and flow straight along the center of the channel, as shown in Fig. 7(b), resulting in separation of blood cells to the upper sub-channel and bacteria into the middle sub-channel (see video in Supplementary Material,† *RBC and bacteria sorting.mpg*), as shown in Fig 7(c).

Fig. 7 Bacteria and blood cells can be effectively separated using this device. (a) The bacteria and blood cells can be focused into a particle stream. (b) When the particles enter into the twDEP electrode array, blood cells experience a higher twDEP force and move towards the upper side wall while the bacteria experiences lower twDEP force and are convected along the center of the channel. (c) This results in a separation with the blood cells flowing into an upper sub-channel downstream and bacteria into a middle sub-channel (see video in Supplementary *RBC and bacteria sorting.mpg*).

As shown previously with cells and bacteria, different sizes of liposomes would exhibit frequency and voltage dependencies for the deflection angle, resulting in different velocities for effective sorting. Liposome sorting is particularly challenging as there is a broad (even multi-modal) distribution involving submicron sizes with small DEP mobility. The liposomes were suspended in deionized water, with a medium conductivity of 2 µS/cm. We applied a voltage of 24 V_{p-p} at a frequency of 3 MHz on the focusing electrode to induce strong nDEP. Particles traveling by the flow will undergo the twDEP force as well as a hydrodynamic force. The large liposomes were repelled away from the electrode array by strong negative DEP, focusing them into a particle stream. The larger liposomes (almost all are larger than 2.7 µm) experienced higher twDEP mobility and were quickly deflected along the co-field direction when an AC field of 12 V_{p-p} and 3 MHz and a flow velocity of roughly 2 mm/sec were applied. Sorting is possible even at this robust linear velocity, corresponding to nearly 6 µl/min. The smaller liposomes (smaller than 2.7 µm) entered into the electrode array and have low twDEP mobility, such that they experience very slow deflection along the co-field direction, resulting in two populations of different size range segregated to different sub-channels, as seen in Fig. 8.

We sorted 100 µl samples into two outlet channels. High purity sorting of particles ranging from 2.1 µm–4.6 µm in size into outlet channel 1 and 0.7 µm–1.8 µm into outlet channel 2 was achieved at a flow rate of 4 µl/min (see video in Supplementary Material†, *Liposome sorting.mpg*). At this flow rate, particles smaller than 700 nm could not be effectively focused and distributed in both of the outlet channels, generating a second size distribution of 380 nm–710 nm in outlet channel 1 and 176 nm–318 nm in the outlet channel 2, following similar size-based sorting trends as the larger particles. Using a higher flow rate of 6 µl/min, effective sorting of particles from 2.3 µm–4.7 µm
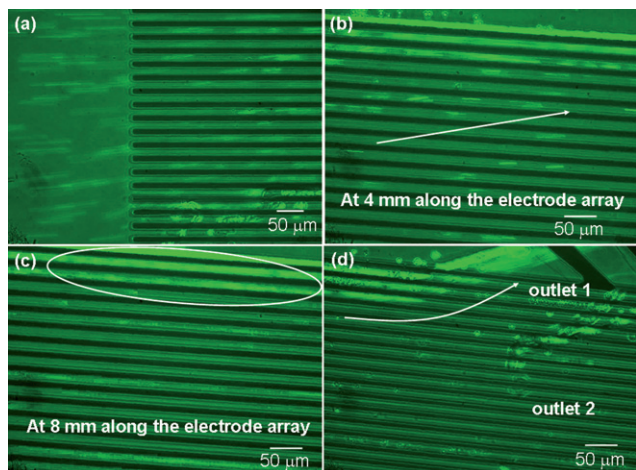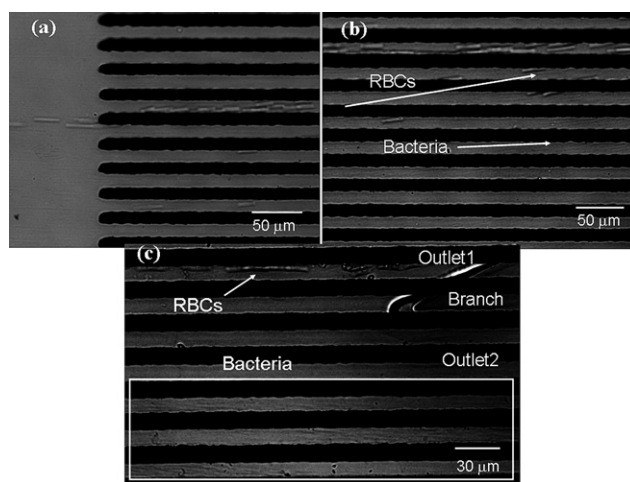

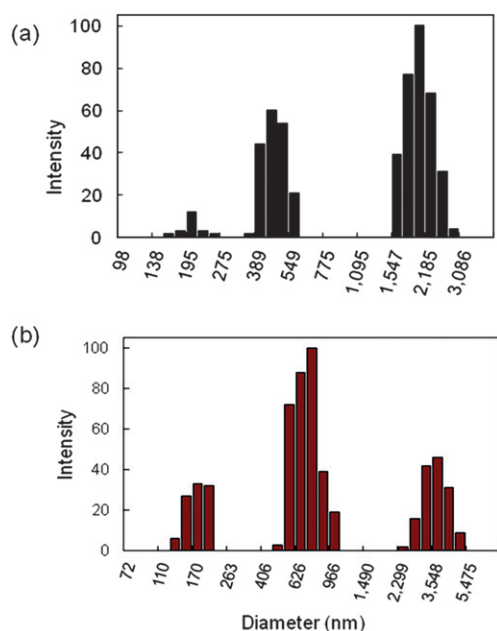Fig. 6 Consecutive images of manipulating RBCs through the array at positions: (a) in front of electrode array, the cells are randomly distributed, (b) sorting begins at 4 mm into the electrode array, (c) at 8 mm into the electrode array almost all the cells have been sorted to the side wall of the channel and are convected towards the upper sub-channel, and (d) cells are sorted into the upper sub-channel at the junction with the main channel.

Fig. 8 Size distribution of sorted liposomes where liposomes of a size ~1–5 μm in diameter were effectively sorted at 6 μl/min into two channels where (a) smaller vesicles (~346–549 nm and ~1.5–2.7 μm) are sorted into channel 1 (b) larger vesicles (~468–965 nm and ~2.3–4.7 μm) are segregated into channel 2. High-purity sorting is achieved for particles larger than one micron because of the geometry of electrode array. The magnitude of the intensity is indicative of the number of liposomes.

in size into outlet channel 1 and 1.5 μm–2.7 μm into outlet channel 2 is achieved, as seen in Fig. 8. Again, small particles are not effectively focused, in this case particles smaller than 1 μm were distributed in both of the outlet channels, generating a second size distribution of 468 nm–965 nm in outlet channel 1 and 346 nm–549 nm in the outlet channel 2, as seen in Fig. 8.

Sorting of sub-micron nanoparticles would require more precise upstream focusing and a smaller electrode gap/width with a reduced wavelength of the traveling field, such that a strong field gradient exists across submicron particles—a good future research topic. The current chip is designed for sorting of micron-sized cells, bacteria and liposomes.

Conclusions

Our experimental results demonstrate that, due to the sustained normal twDEP force provided by an internal array, sorting of micron-sized particles can be achieved in an integrated DEP chip at linear velocities exceeding mm/sec and flow rates near 10 μl/min. Red blood cells are observed to move along the co-field direction in a narrow frequency range of 300 kHz to 650 kHz and are concentrated into downstream subchannels. Blood cells and bacteria also have been focused, manipulated and separated successfully but at a lower flow rate. A broadly distributed liposome sample has been sorted into distinct size ranges at very high linear velocities of several mm/s and flow rates approaching 10 μl/min, despite their smaller size. The device can hence sort different species, as well as different sized cells of the same species. Unlike many other devices, cells in our device are

generally repelled away from the chip surface by choosing a field frequency which creates a negative DEP force, so that cell sticking and lysing can be avoided. The high throughput microsorter has great potential to provide fast and portable diagnostics, as a 10 μl/min throughput translates into a 10 minute sorting time for a typical 100 μl sample in a palm-sized device. Extension to high-throughput portable sorting of sub-micron particles is also discussed.

References

1 S. Miltenyi, W. Müller, W. Weichel and A. Radbruch, *Cytometry*, 1990, **11**, 231.
2 J. J. Chalmers, M. Zborowski, L. Sun and L. Moore, *Biotechnol. Prog.*, 1998, **14**, 141.
3 A. Y. Fu, C. Spence, A. Scherer, F. H. Arnold and S. R. Quake, *Nat. Biotechnol.*, 1999, **17**, 1109.
4 S. F. Ibrahim and G. van den Engh, *Curr. Opin. Biotechnol.*, 2003, **14**, 5.
5 H. A. Pohl, *Dielectrophoresis*, 1978, (Cambridge: Cambridge University Press).
6 H. Li and R. Bashir, *Sens. Actuators, B*, 2002, **86**, 215.
7 Z. Gagnon and H. C. Chang, *Electrophoresis*, 2005, **26**, 3725.
8 J. Gordon, Z. Gagnon and H. C. Chang, *Biomicrofluidics*, 2007, **1**, 044102.
9 Z. Gagnon, S. Senapati and H. C. Chang, *Electrophoresis*, 2008, **29**, 4808.
10 L. Wang, L. A. Flanagan, N. L. Jeon, E. Monuki and A. P. Lee, *Lab Chip*, 2007, **7**, 1114.
11 P. Gascoyne, C. Mahidol, M. Ruchirawat, J. Satayavivad, P. Watcharasit and F. F. Becker, *Lab Chip*, 2002, **2**, 70.
12 X. B. Wang, J. Yang, Y. Huang, J. Vykoukal, F. F. Becker and P. R. Gascoyne, *Anal. Chem.*, 2000, **72**, 832.
13 S. Fiedler, S. G. Shirley, T. Schnelle and G. Fuhr, *Anal. Chem.*, 1998, **70**, 1909–1915.
14 X. Hu, P. H. Bessette, J. Qian, C. D. Meinhart, P. S. Daugherty and H. T. Soh, *Proc. Natl. Acad. Sci. U. S. A.*, 2005, **102**, 15757.
15 D. F. Chen, H. Du and W. H. Li, *J. Micromech. Microeng.*, 2006, **16**, 1162.
16 I. F. Cheng, D. Hou, H.-C. Chang and H.-C. Chang, *Biomicrofluidics*, 2007, **1**, 021503.
17 S. Masuda, M. Washizu and M. Iwadare, *IEEE Trans. Ind. Appl.*, 1987, **23**, 474.
18 G. Fuhr, R. Hagedorn, T. Muller, W. Benecke, B. Wagner and J. Gimsa, *Studia Biophys.*, 1991, **140**, 79.
19 X. B. Wang, Y. Huang, F. F. Becker and P. R. Gascoyne, *J. Phys. D: Appl. Phys.*, 1994, **27**, 1571.
20 M. P. Hughes, R. Pethig and X. B. Wang, *J. Phys. D: Appl. Phys.*, 1996, **29**, 474.

21 H. Morgan, A. G. Izquierdo, D. Bakewell, N. G. Green and A. Ramos, *J. Phys. D: Appl. Phys.*, 2001, **34**, 1553.
22 Y. Huang, X. B. Wang, J. A. Tame and R. Pethig, *J. Phys. D: Appl. Phys.*, 1993, **26**, 1528.
23 M. S. Talary, J. P. Burt, J. A. Tame and R. Pethig, *J. Phys. D: Appl. Phys.*, 1996, **29**, 2198.
24 G. De Gasperis, J. Yang, F. F. Becker, R. C. Peter Gascoyne and X. B. Wang, *Biomed. Microdevices*, 1999, **2**, 41.
25 H. Morgan, N. G. Green, M. P. Hughes, W. Monaghan and T. C. Tan, *J. Micromech. Microeng.*, 1997, **7**, 65.
26 L. Cui and H. Morgan, *J. Micromech. Microeng.*, 2000, **10**, 72.
27 X. B. Wang, Y. Huang, X. Wang, F. F. Becker and P. R. Gascoyne, *Biophys. J.*, 1997, **72**, 1887.
28 R. Pethig, M. S. Talary and R. S. Lee, *IEEE Engineering in Medicine and Biology Magazine*, 2003, **22**, 43.
29 T. Sun, H. Morgan and N. G. Green, *Phys. Rev. E*, 2007, **76**, 046610.
30 A. Ramos, H. Morgan, N. G. Green, A. Gonzalez and A. Castellanos, *J. Appl. Phys.*, 2005, **97**, 084906.
31 V. E. Froude and Y. Zhu, *J. Phys. Chem. B*, 2009, **113**, 1552.
32 D. D. Lasic, *Tibtech*, 1998, **16**, 307.